Quantifying and attributing methane emissions from coal mine aggregation areas using high-frequency ground-based observations

Fan Lu[1], Kai Qin[1*], Jason Blake Cohen[1*], Qiansi Tu[2], Chang Ye[1], Yanan Shan[1], Pravash Tiwari[1], Qin He[1], Qing Xu[1], Shuo Wang[1]

[1]*Jiangsu Key Laboratory of Coal-Based Greenhouse Gas Control and Utilization, School of Environment and Spatial Informatics, China University of Mining and Technology, Xuzhou, China*

[2]*School of Mechanical Engineering, Tongji University, Shanghai, China*

Abstract This work introduces the results of an intensive 15-day surface observation campaign of methane (CH_4) and adapts a new analytical method to compute and attribute CH_4 emissions. The selected area has a high atmospheric concentration of CH_4 (campaign-wide minimum/mean/standard deviation/max observations: 2.0, 2.9, 1.3, and 16 ppm) due to a rapid increase in the mining, production, and use of coal over the past decade. Observations made in concentric circles at 1km, 3km, and 5km around a high production high gas coal mine were used with the mass conserving model free emissions estimation approach adapted to CH_4, yielding emissions of 0.73, 0.28, and 0.15 ppm/min respectively. Attribution used a 2-box mass conserving model to identify the known mine's emissions from 0.042-5.3 ppm/min, and a previously unidentified mine's emission from 0.22-7.9 ppm/min. These results demonstrate the importance of quantifying the spatial distribution of methane in terms of control of regional-scale CH_4 emissions.

Key Points

1.) Campaign-wide CH_4 observations show a mean concentration of 2.9 ppm and a maximum of 16 ppm, indicating very high coal mine emissions.
2.) Computed CH_4 emissions decreased away from the mine, from 0.73 ppm/min at 1km to 0.15 ppm/min at 5km, indicating wide spatial impact.
3.) Emissions attributed to known mine (0.042-5.3 ppm/min) and unknown mine (0.22-7.9 ppm/min), allowing better regional emissions control.

Plain Language Summary The study measures methane levels around a high production and

high gas coal mine and finds very high concentrations, averaging 2.9 ppm and reaching 16 ppm compared to the global background of 1.8-1.9 ppm. Emissions were estimated using a new model free mass conserving approach at different distances from the mine, and found to decrease from 0.73 ppm/min 1 km away from the mine to 0.15 ppm/min 5 km away from the mine. Attribution however identified two separate sources, with the known mine having a range of emissions from (0.042-5.3 ppm/min) and a second previously unknown mine with a range of emissions from (0.22-7.9 ppm/min). This work shows the importance of measuring methane at both high temporal frequency and simultaneously over a well-sampled set of spatial coordinates across the area of interest, quantify emissions from different sources. It is hoped that this approach can better identify and quantify methane leakage from coal mining, and allow for more precise control.

Key Words: *CH_4; Top-down emissions; Mass-conserving Model; Attribution; Mining*

1. Introduction

Emissions of Methane [CH_4] contribute the second most to direct anthropogenic longwave radiative forcing (Etminan et al., 2016; Li et al., 2022). Since CH_4 has a lifetime from 9.5 to 12.5 years (Li et al., 2022; Prather et al., 2012), controlling methane emissions can provide an opportunity to mitigate peak loading and slow the rate of net global warming (Nature, 2021).

Fossil fuel CH_4 is one of the largest sources of anthropogenic methane emissions (Kirschke et al., 2013; Saunois et al., 2020a). Since China is the world's largest producer and consumer of coal (Bournazian, 2016), CH_4 emitted fro coal mines [CMM] possibly contributes up to 33%-40% of China's total CH_4 emissions (Janssens-Maenhout et al., 2017; Miller et al., 2019; Peng et al., 2016). Although China enacted CMM regulations in 2010 (Kerr and Yang, 2009), CMM continues grow (Miller et al., 2019).

Methane emission estimates are highly uncertain (Brandt et al., 2014; Saunois et al., 2020b) in both space and time. They also generally have a fat tail distribution, wherein a small number of samples have extremely large emissions that overwhelm emissions under average conditions (Duren et al., 2019; Plant et al., 2022). For these reasons, new approaches to quantify, reduce uncertainty, and attribute CH_4 emissions can provide support for policies aiming to control and mitigate CMM (Cao, 2017).

Bottom-up (BU) quantification of emissions requires a priori knowledge of source locations and diversity, which tends to not represent real-world conditions. Top-down (TD) approaches analyze concentration data with improving accuracy (Allen, 2014; Rigby et al., 2019; Varon et al., 2018; Vaughn et al., 2018), specifically combining surface (Heerah et al., 2021; Katzenstein et al., 2003; Shi et al., 2023), aircraft (Karion et al., 2013; Shi et al., 2022; Tong et al., 2023; Vinković et al., 2022), and/or satellite (Wecht et al., 2014) CH_4 observations with atmospheric models. Some TD approaches use physically realistic but complex chemical transport models (Bloom et al., 2017) , others use plume models (Goldsmith et al., 2012), and others still use data driven approaches (Buchwitz et al., 2017). Uncertainties are rarely assessed holistically or in detail (Cohen and Prinn, 2011; Cohen and Wang, 2014).

Airborne remote sensing is a highly technical and costly approach to record CH_4 fluxes from landfills, coal basins, and oil and gas production (Krautwurst et al., 2021; Krautwurst et al., 2017; Kuhlmann et al., 2023), which suffers from not being able to monitor CH_4 emissions over long periods

of time or in regions where the source is not well constrained (Brandt et al., 2014; Gorchov Negron et al., 2020; Hiller et al., 2014; Mehrotra et al., 2017; Molina et al., 2010). Satellite remote sensing can measure CH_4 under specific orbits where the source is known and identified (Jacob et al., 2016; Jacob et al., 2022; Plant et al., 2022; Varon et al., 2018; Zhang et al., 2020), but only after being calibrated by upward looking remotely sensed measurements (Tu et al., 2022), and only when the atmosphere is rain, cloud and aerosol free (Cohen and Prinn, 2011; Reuter et al., 2019; Sadavarte et al., 2021). TROPOMI and GOSAT have both been shown to be data-rich at times (Butz et al., 2012; Hu et al., 2018; Jacob et al., 2016), but severely limited at other times (Butz et al., 2012; Kuze et al., 2009). Even when these satellites have sufficient data to compute emissions from other species, frequently CH_4 cannot be computed (Li et al., 2023; Qin et al., 2023b) due to insufficient signal strength, and uncertainties which are both non-understood and mis-constrained (Povey and Grainger, 2015).

Ground-based remote sensing provides higher accuracy versus satellite observations (Heerah et al., 2021; Luther et al., 2022; Tu et al., 2022). EM27/SUN measurements have approximated CH_4 emissions in Poland (Luther et al., 2019; Luther et al., 2022). However, these instruments are expensive, require calibration, and have limited data collection due to solar signal strength.

This work employs a high-frequency surface-based observation platform of CH_4 concentration which is portable, economical, and unaffected by most environmental factors. The observations are combined with a new mass-conserving methodology based on temporal transformation of the spatially derived mass-conserving framework successfully applied to NO_2 (Li et al., 2023; Qin et al., 2023b). This work focuses on Shanxi, one of the densest coal mining regions in the world, accounting for approximately 10% of total global coal production (Lin and Liu, 2010; Qin et al., 2023a). Continuous observations were made around known coal mines, unknown sources, and of background conditions. High-frequency emissions calculated using these data were used to drive a 2-box model to attribute emissions to the known mine and a second low production mine previously thought insignificant. The results provide insights into the spatial distribution of CH_4 emissions, demonstrate rapid adoption of practical methods globally, and enable source attribution.

2. Method and Data

2.1. Study Site and Campaign Design

Changzhi, Shanxi is located in a basin, with coal mines densely distributed throughout both flat central regions and around the mountainous edges (Figure S1), many of which are classified as high

CH_4 emitting mines. Due to this combination, province-wide background CH_4 concentrations are very high and have large variation in time. One mine is classified as having high amounts of CH_4 per unit of production and an annual coal production of 4 million tons [CM-A], and the other is unclassified for CH_4 per unit of production and having an annual coal production of 3 million tons [CM-B] (Qin et al., 2023a). Observations were positioned along concentric circles located 1km, 3km, and 5km from CM-A, over an approximation of the four ordinal directions: east, west, south, north (Figure1). All locations were planned to be far away from known anthropogenic sources, leading to a net total 12 measurement points. As later discovered, CM-B is located approximately 1km southwest from the measurement point located at 5km west.

2.2. Measuring CH_4 Concentration

CH_4 concentrations were observed daily at 1 Hz from 8:30 to 17:00 local time in August 2022 using a portable greenhouse gas analyzer (LGR-915-0011, California, USA) 5m above the surface. Three different locations were selected daily along a single ordinal direction from the mine center, allowing a more consistent and precise calculation of the spatial gradient (Table S1). The CH_4 data was averaged minute-by-minute to match observed wind data, and subsequently used to compute emissions. As show in Figure S2, the CH_4 concentration data is highly correlated with rapid changes in both the wind speed and direction.

Observations made in clean locations with a wind direction not from the mine are subsequently considered for background sites. The lowest and least variable CH_4 observations are found on August 23 in the south (2.08ppm±0.08) (Figure S2). It is important to note that although the minimum in this work, these values are significantly higher than the global latitude-band background. Three other locations and days were observed with relatively low mean and not significantly large variation: August 19 in the east (2.63ppm±0.35), August 22 in the east (2.65ppm±0.51), and August 22 in the south (2.60ppm±0.55) (Figure S2). These results imply that the practice adopted by the community to separate a plume from the global latitude band or climatological background state is not applicable in the locations sampled in this paper (Buchwitz et al., 2017; Irakulis-Loitxate et al., 2021; Lauvaux et al., 2022; Sadavarte et al., 2021). For this reason, a new quantitative approach is presented to understand and quantify what is actually a source and what is not. This approach is applicable under conditions both encountered globally as well as those under the uniquely high and variable conditions observed herein.

157 **2.3. Meteorological Data**

158 The wind speed and direction were obtained from local meteorological stations with a temporal
159 frequency of 1min. As show in Figures S3 and S4 the overall wind was dominated by a southerly
160 direction (38.0% of observations between 150° and 210°) and found to be moderately slow (69.9% of
161 observations were between 1 m/s and 4 m/s). The 10th and 90th percentiles of wind direction (54° and
162 312°) and wind speed (1 m/s and 5.1 m/s) respectively, indicate that high frequency sampling reveals a
163 small number of relatively large changes are observed, which are expected to lead to a "fat-tail" type of
164 distribution of subsequently computed emissions (Delkash et al., 2016).

165 **2.4. Quantitative Estimation of CH_4 Emissions**

166 A mass conserving approach was used to estimate the CH_4 emissions in connection with the high
167 frequency observations of CH_4 and meteorological data, hereafter called the Mass Conserving Model
168 of Measured Coal Methane [MCM^2]. This approach is based on previous emissions estimates of total
169 atmospheric column observations of short-lived NO_x (Li et al., 2023; Qin et al., 2023b), but has never
170 been applied to surface observations in general, or CH_4 in specific. Adopting this approach methane is
171 done starting with mass conservation (Equation 1), and reorganizing the individual terms (Equations 2,
172 3) as follows:

$$\frac{\partial CH_4}{\partial t} = E_{CH_4} - \alpha \times \nabla(U \times CH_4) \qquad (1)$$

$$\nabla(U \times CH_4) = CH_4 \times \frac{\partial U}{\partial t} + U \times \frac{\partial CH_4}{\partial t} \qquad (2)$$

$$\frac{\partial CH_4}{\partial t} = E_{CH_4} - \alpha \times \left(CH_4 \times \frac{\partial U}{\partial t} + U \times \frac{\partial CH_4}{\partial t}\right) \qquad (3)$$

173 where CH_4 is methane concentration (ppm), t is time (min), E_{CH_4} is CH_4 emissions (ppm/min), α is a
174 conversion coefficient between distance and wind speed, and U is wind speed (m/s).

175 Uncertainty analysis was conducted before calculating the CH_4 emissions to ensure only reliable data
176 was used, since observed variation of CH_4 over time is influenced not only by CH_4 emissions, but also
177 changes in wind speed and pressure. Specifically, $CH_4 \times \frac{\partial U}{\partial t}$ represents the change in CH_4 influenced
178 by pressure, while $U \times \frac{\partial CH_4}{\partial t}$ represents the change in CH_4 influenced by advection. Furthermore, since
179 there is uncertainty in the observations, this work takes a conservative approach, and only considers
180 data when the threshold given by equation (4) is observed to be considered influenced by emissions.

$$u \times \frac{\partial CH_4}{\partial t} / \nabla(U \times CH_4) > 30\% \quad (4)$$

181 The remaining data (approximately 22%, Figure S5) is not processed in the emissions calculation as the

signal is most likely due to a combination of observational uncertainty and white noise (Prinn et al., 1987).

2.5. Attribution Analysis

A 2-box mass conserving model (based on equation 5) was used to attribute emissions from the more than one suspected source of CH_4 in the west. The change in CH_4 over time t (min) at the observation point $C_{coal\ mine}$ (ppm) is driven by Emissions from the upwind coal mine $E_{coal\ mine}$ (ppm/min) and the concentration gradient computed using the wind U (min^{-1}), and the background concentration $C_{background}$ (ppm) as demonstrated in (Figure S6).

$$\frac{\partial C_{coal\ mine}}{\partial t} = E_{coal\ mine} + U \times C_{background} - U \times C_{coal\ mine} \qquad (5)$$

All observed individual data points and computed emissions are used wind direction is capable of transporting the CH_4 from either CM-A or CM-B towards the observation site, while the remaining data is not used. A discretized version of Equation 5 is given in Equation 6 and solved using a first order finite difference approach:

$$C_{Coal\ mine_{\tau i+1}} - C_{coal\ mine_{\tau i}} = E_{coal\ mine_{\tau i}} + U_{\tau i} \times C_{background_{\tau i}} - U_{\tau i} \times C_{coal\ mine_{\tau i}} \qquad (6)$$

where τ_i and τ_{i+1} are the current and next time step, and the other terms are defined as in equation 5.

All possible sets of steady-state concentrations are computed using all possible combinations of emissions and concentrations as boundary and initial conditions and running the equation forward to equilibrium. The computed concentrations are analyzed probabilistically by comparing the modeled CH_4 probability density function (PDF) with the observed CH_4 PDF. Differences between the PDFs are clearly associated with the different wind directions and hence geophysical locations of the sources can be distinguished.

3. Results and Discussion

3.1. Observations and Analysis of CH_4 Concentration

Time series of CH_4 concentration, wind speed, and direction at 1km, 3km and 5km north of CM-A are given in Figure 2. The wind direction blew from CM-A towards the observations (between 150° and 210°) 59.2% of the time, with only one day observed at 1km north (August 15) with a significant amount of wind from the west (between 240° and 300°). Consistent with CM-A being the major source at 1km, when the wind blew from the south, the CH_4 concentration (3.45±0.79) was both higher and had a larger variation than when the wind blew from the west (2.40±0.17) which was similar to background conditions. This is consistent with there being no known significant sources to the west from this observation location, as shown in Figure 1. Similarly, under faster than average wind

conditions from the direction of CM-A (On August 21 the mean wind was 5.70 m/s with 14.9% of observations faster than 7 m/s), the observed concentrations were slightly lower, yet similarly variable (3.17±0.82). All of these findings are consistent with transport dominating the concentrations at 1km north, and that high frequency wind and concentration observations are required in tandem to compute the required spatial gradients in the CH_4, otherwise there is no basis to objectively separate the effects of the emitting region (CM-A) from the background.

A similar set of findings were observed at 3km north, while 5km north is generally similar to the background. At 3km north, when the wind was from the south (59.3% of data), the concentration was lower and more variable (3.16±1.48, with 78.7% of observations below 3.0ppm) than at 1km north, consistent with advection from CM-A and a relatively stable atmosphere with a small contribution from diffusion between the plume and the background. When the wind blew from other directions, the distribution of concentrations broadened considerably, with a range from background (2.25ppm) through extremely polluted (16.2ppm). One subset of this was observed on August 15 (observed over a total of 61 mins of observations, 6.68% of the total observations at 3km north) when the wind was from the west and slow, where the concentration was (5.44±2.82), as depicted in Figure 2. The data on this day aligned with the presence of a major highway west of the observation site, which was observed in-person to have heavy traffic consisting of vehicles carrying coal (which could still be outgassing) as well as others powered by CNG. At 5km north the overall concentration (2.40±0.28) was generally lower than at 3km and had much lower variability, consistent with background CH_4.

Time series of CH_4 measured at 1km, 3km and 5km west of CM-A and corresponding wind direction and speed are given in Figure 2. Overall, the main wind direction is from the south 98.4% of the time at 1km, 74.5% of the time at 3km, and 70.2% of the time at 5km, and the wind speed was very high when measuring CH_4 at 1km west, with an average value of 4.28±1.13m/s and a maximum of 7.4m/s. This set of findings is consistent with clean upwind sources. Accordingly at 1km west, the observed CH_4 was slightly higher than background and had similar variability to 1km and 3km north (2.71±0.94ppm and 86.5% of the data below 3ppm). At 3km west, CH_4 was observed to be similar to the background (2.32±0.09ppm). The only exception was found at 1km west between 9:00 am and 9:30 am on August 17, in which all of the observations were greater than 4ppm. Since the areas to the west from 1km west contains mostly farmland, there was no expected strong source of CH_4, as shown in Figure 1. This indicates that during this special short time, the observed slow increase and rapid fall-off in CH_4

concentration must be due an unidentified source, or a change in the boundary layer and/or vertical mixing structure.

Following this, it was anticipated that the 5km west site would exhibit background types of conditions, however the observed data deviates significantly. Wind speed was low (1.63±0.54m/s, maximum 3.0 m/s),CH_4 was both very high and exhibited substantial temporal variability (5.83±2.99 ppm, 66.7% exceeding 4ppm, and peak of 15.3 ppm), and 70.2% of the observations were from the south as demonstrated in (Figure 2). From Figure 1, it can be seen that there is another Coal mine (hereafter CM-B) located about 1km away from the 5km west measurement point, to its southwest, although CM-B has an annual production of about 3 million tons (smaller than CM-A) and not considered to be high gas (like CM-A), and therefore was not previously considered important. The overlap of high concentrations with low a priori emissions, suggests that formal attribution is essential to quantitatively confirm whether CM-B is the source responsible for both typical conditions at 5km west, as well as the long-range transport event at 1km west.

CH_4 concentrations and wind observations in all directions except to the west, and except for the small number of special events documents above, exhibit PDFs that show there is a decrease in concentration the further the distance from CM-A (Figures S7 and S8), indicating that CM-A is consistent with the major sources in these regions. These decreases are observed in terms of the median, mean, distribution width, and percentage over 4.0ppm all decreasing from 1km north to 3km north and again from 3km north to 5km north.

The observed CH_4 concentration gradient as one moves westward from CM-A is inconsistent with the other ordinal directions (Figure S7). While there was a small decrease in the mean and distribution breadth from 1km west to 3km west, there was a large increase in the median, mean, distribution width, percentatge over 4.0ppm from 3km west to 5km west. Furthermore, the data at 5km west was found to be skewed differently than at the other sites, with approximately 70% of the data greater than 4.0ppm. The data clearly indicates that the 5km west site behaves more like a source region than even the 1km north site.

3.2. Quantification and Characteristics of CH_4 Emissions

The emissions have been computed at each following Equations 3 and 4, with 25.7% of observations yielding emissions results. The PDFs of the emissions (Figures 3 and S9) reveal that the three stations in the north and the 5km west station all are relatively high and variable, while the remainder are

relatively low and non-variable. Among all the CH_4 emissions results, the highest median, mean, maximum, and breadth of the distribution are all observed at 5km west. The 3km south location has the lowest emissions of all points observed (by median), with a respective median, mean, maximum, and percentage greater than 1.0ppm/min of (0.03ppm/min, 0.26ppm/min, 0.90ppm/min, 0%) (Figure S9), and is subsequently considered representative of background emissions in this work. It is important to note that there is no area within this region that has 0ppm/min emissions and that the minimum concentration on average is about 2.23ppm (Figure S8), both of which are considered very high or polluted compared with most other current studies (Irakulis-Loitxate et al., 2021; Sadavarte et al., 2021).

The spatial distribution of the CH_4 emissions is similar to that of the CH_4 concentration observations (Figure 3). First, there is a decrease as one moves northward along the axis away from CM-A, with the median, mean, maximum, and percentage of emissions greater than 1.0ppm/min at 1km north (0.73ppm/min, 1.18ppm/min, 5.67ppm/min, and 42%) all larger than at 3km north (0.28ppm/min, 0.72ppm/min, 3.41ppm/min, and 29%). The values at 3km north are also larger than those at 5km north, which respectively are (0.11ppm/min, 0.18ppm/min, and 0.59ppm/min, and 0%). The subset of emissions under low wind speed conditions exhibited a larger decline from 1km to 3km and from 3km to 5km. The observations are further consistent with transport from a single dominant source located at CM-A being the primary driving factor, and diffusion from other industrial sources in Changzhi city center being a secondary factor.

Consistent with there being few to no sources impacting the 1km west and 3km west sites, except for considerably less transport from CM-A the computed PDFs at these sites (Figure 3) demonstrate low emissions and low variability, with the respective median, mean, maximum, and percentage of emissions greater than 1.0ppm/min at 1km west being (0.28ppm/min, 0.55ppm/min, 3.03ppm/min, and 16%) and at 3km west being even lower (0.08ppm/min, 0.10ppm/min, 0.27ppm/min, and 0%). However, the CH_4 emissions computed at 5km west were the highest and most variable of all results computed in this work, with the respective statistics being (1.45ppm/min, 1.82ppm/min, 7.92ppm/min, and 60%). Furthermore, the skewness of the distribution at 5km west (which has 30% of the CH_4 emissions above 2.0ppm/min) is much larger than at 1km north (which only has 15% of emissions above 2.0ppm/min). Combining these pieces of information, at first look it seems that the site at 5km west is not related to the emissions from CM-A, or at best are a mixture of emissions from CM-A and

those at another site, herein proposed to be CM-B. The remainder of this study focuses on disentangling and attributing contributions from CM-A and CM-B at 5km west, with the observations at the remaining sites ruled out in terms of having a contribution from CM-B.

3.3. Attribution of Emissions

This works applied the 2-box model at the 5km west site and quantified the contribution of both CM-A and CM-B emissions to the observed CH_4 concentration distributions as given in Figure 3. First, the results of the 2-box model produce PDFs which overlap with the overall observed CH_4 PDF, indicating that the results are reasonable. Second, space of the emissions computed from the two different two coal mines do not overlap, and cover two independent portions of the observed CH_4 PDF. Specifically, the observed CH_4 concentrations as a whole have a 30%, 50%, and 70% value of (3.68ppm, 5.18ppm, and 6.86ppm) respectively. The emissions from CM-A yield a CH_4 concentration less than 4ppm most of the time, with a 30%, 50%, 70%, and maximum concentration of (2.96ppm, 3.15ppm, 3.31ppm, and 4.60ppm), while the emissions from CM-B yield a CH_4 concentration more than 5ppm most of the time, with a minimum, 30%, 50%, 70%, and maximum concentration of (4.76ppm, 5.20ppm, 5.68ppm, and 6.18ppm).

Overall, the emissions from CM-B cover well the observed concentration values from the range of 50% to 70%, with a single high value around the 90% value, while the emissions from CM-A cover well the observed concentration values in the range from 10% to 30%. One weakness is that the length of observations is not as comprehensive as at the other sites, and therefore it is possible that had more observations been made, the contributions from CM-B would have filled more of the space between the 70% and 90% levels, and some combination of sources from CM-A and CM-B would have better filled the space between the 30% and 50% levels. Overall, the results indicate to a high degree of certainty that the emissions from the two respective coal mines are distinct, with CM-A the source of emissions in the lower range of the concentration distribution and CM-B the source for emissions in the higher concentration range, covering values in the middle and upper range. Improvements in modeling, additional observations, considering possible contributions from additional missing sources, and consideration of longer-range transport could add further improvement and better explore the intermediate range of observed concentrations.

4. Conclusions

This work demonstrates that high frequency surface observations of CH_4, in combination with high

frequency observations of wind can provide deep insights into emissions by accounting for high frequency changes in space and time at the same time, which tend to be missing from models which used more idealized approaches (such as average plume shapes and sizes, levels of coal production, and interpreting gradients from a small number of fixed images). This work demonstrates that a significant source of CH_4 emissions from a previously unknown or improperly classified mine may pose a vastly different range of observed concentration as well as computed emissions than expected. The importance of observations at both high frequency and regional spatial coverage are demonstrated, and a set of practical methods that are freely open and can be adopted and modified rapidly are provided. The approach to source attribution used herein can provide insights to policymakers to formulate regional emission control policies and provide a check on or a priori assumption for the new generation of advance satellite-based top-down emissions estimates, while demonstrating that spatial attribution is a critical next-step for satellite approximations and methane control policies.

Acknowledgments

This study was funded by the National Nature Science Foundation of China (42075147, 42375125), the Fundamental Research Funds for the Central Universities (2023KYJD1003). We sincerely appreciate all the scientists, engineers, and students who participated in the field campaigns, maintained the measurement instruments, and helped with and collection and processing of the data.

K.Q., J.B.C. and F.L. designed the research; F.L., C.Y., and Y.S. collected the data; J.B.C. and F.L. analyzed the data; Q.T. and Q.X. provided the support for data analysis and drawing; Q.H., S.W gave suggestion on running the 2-Box model; F.L. wrote the manuscript with inputs from J.B.C. and P.T.; All authors discussed the results and contributed to the final manuscript.

Open Research

Data Availability Statement

All underlying data herein are available for access by the editors and reviewers at https://figshare.com/s/1a393772d7b72ae17e62 and will be made available to the community upon publication.

References

Allen, D. T. (2014). Methane emissions from natural gas production and use: reconciling bottom-up and top-down measurements. *Current Opinion in Chemical Engineering*, 5, 78-83. https://doi.org/10.1016/j.coche.2014.05.004

Bloom, A. A., Bowman, K. W., Lee, M., Turner, A. J., Schroeder, R., Worden, J. R., et al. (2017). A

global wetland methane emissions and uncertainty dataset for atmospheric chemical transport models (WetCHARTs version 1.0). *Geosci. Model Dev,* 10 (6), 2141-2156. https://doi.org/10.5194/gmd-10-2141-2017

Bournazian, J. (2016). US. Energy Information Administration. https://hdl.handle.net/1813/45040

Brandt, A. R., Heath, G. A., Kort, E. A., O'Sullivan, F., Pétron, G., Jordaan, S. M. et al. (2014). Methane Leaks from North American Natural Gas Systems. *Science*,343 (6172), 733-735. DOI:10.1126/science.1247045

Buchwitz, M., Schneising, O., Reuter, M., Heymann, J., Krautwurst, S., Bovensmann, H. et al. (2017). Satellite-derived methane hotspot emission estimates using a fast data-driven method. *Atmos. Chem. Phys.,*17 (9), 5751-5774. https://doi.org/10.5194/acp-17-5751-2017

Butz, A., Galli, A., Hasekamp, O., Landgraf, J., Tol, P., & Aben, I. (2012). TROPOMI aboard Sentinel-5 Precursor: Prospective performance of CH_4 retrievals for aerosol and cirrus loaded atmospheres. *Remote Sensing of Environment*, 120, 267-276. https://doi.org/10.1016/j.rse.2011.05.030

Cao, X. (2017). Policy and regulatory responses to coalmine closure and coal resources consolidation for sustainability in Shanxi, China. *Journal of Cleaner Production*, 145, 199-208. https://doi.org/10.1016/j.jclepro.2017.01.050

Cohen, J. B., & Prinn, R. G. (2011). Development of a fast, urban chemistry metamodel for inclusion in global models. *Atmos. Chem. Phys.*, 11 (15), 7629-7656. https://doi.org/10.5194/acp-11-7629-2011

Cohen, J. B., & Wang, C. (2014). Estimating global black carbon emissions using a top-down Kalman Filter approach. *Journal of Geophysical Research: Atmospheres*, 119 (1), 307-323. https://doi.org/10.1002/2013JD019912

Delkash, M., Zhou, B., Han, B., Chow, F. K., Rella, C. W., & Imhoff, P. T. (2016). Short-term landfill methane emissions dependency on wind. *Waste Management*, 55, 288-298. https://doi.org/10.1016/j.wasman.2016.02.009

Duren, R. M., Thorpe, A. K., Foster, K. T., Rafiq, T., Hopkins, F. M., Yadav, V. et al. (2019). California's methane super-emitters. *Nature*, 575 (7781), 180-184. https://doi.org/10.1038/s41586-019-1720-3

Etminan, M., Myhre, G., Highwood, E. J., & Shine, K. P. (2016). Radiative forcing of carbon dioxide, methane, and nitrous oxide: A significant revision of the methane radiative forcing. *Geophysical Research Letters*, 43 (24), 12,614-612,623. https://doi.org/10.1002/2016GL071930

Goldsmith, C. D., Chanton, J., Abichou, T., Swan, N., Green, R., & Hater, G. (2012). Methane emissions from 20 landfills across the United States using vertical radial plume mapping. *Journal of the Air & Waste Management Association*, 62 (2), 183-197. https://doi.org/10.1080/10473289.2011.639480

Gorchov Negron, A. M., Kort, E. A., Conley, S. A., & Smith, M. L. (2020). Airborne Assessment of Methane Emissions from Offshore Platforms in the U.S. Gulf of Mexico. *Environmental Science & Technology*, 54 (8), 5112-5120. https://doi.org/10.1021/acs.est.0c00179

Heerah, S., Frausto-Vicencio, I., Jeong, S., Marklein, A. R., Ding, Y., Meyer, A. G. et al. (2021). Dairy Methane Emissions in California's San Joaquin Valley Inferred With Ground-Based Remote Sensing Observations in the Summer and Winter. *Journal of Geophysical Research: Atmospheres*, 126 (24), e2021JD034785. https://doi.org/10.1029/2021JD034785

Hiller, R. V., Neininger, B., Brunner, D., Gerbig, C., Bretscher, D., Künzle, T. et al. (2014). Aircraft-based CH_4 flux estimates for validation of emissions from an agriculturally dominated area in Switzerland. *Journal of Geophysical Research: Atmospheres*, 119 (8), 4874-4887.

https://doi.org/10.1002/2013JD020918

Hu, H., Landgraf, J., Detmers, R., Borsdorff, T., Aan de Brugh, J., Aben, I. et al. (2018). Toward Global Mapping of Methane With TROPOMI: First Results and Intersatellite Comparison to GOSAT. *Geophysical Research Letters*, 45 (8), 3682-3689. https://doi.org/10.1002/2018GL077259

Irakulis-Loitxate, I., Guanter, L., Liu, Y.-N., Varon, D. J., Maasakkers, J. D., Zhang, Y. et al. (2021). Satellite-based survey of extreme methane emissions in the Permian basin. *Science Advances*, 7 (27), eabf4507. DOI: 10.1126/sciadv.abf4507

Jacob, D. J., Turner, A. J., Maasakkers, J. D., Sheng, J., Sun, K., Liu, X. et al. (2016). Satellite observations of atmospheric methane and their value for quantifying methane emissions. *Atmos. Chem. Phys.*, 16 (22), 14371-14396. https://doi.org/10.5194/acp-16-14371-2016

Jacob, D. J., Varon, D. J., Cusworth, D. H., Dennison, P. E., Frankenberg, C., Gautam, R. et al. (2022). Quantifying methane emissions from the global scale down to point sources using satellite observations of atmospheric methane. *Atmos. Chem. Phys.*, 22 (14), 9617-9646. https://doi.org/10.5194/acp-22-9617-2022

Janssens-Maenhout, G., Crippa, M., Guizzardi, D., Muntean, M., & Petrescu, A. M. R. (2017). EDGAR v4.3.2 Global Atlas of the three major Greenhouse Gas Emissions for the period 1970–2012. *Earth System Science Data Discussions*, 1-55. https://doi.org/10.5194/essd-2017-79

Karion, A., Sweeney, C., Pétron, G., Frost, G., Michael Hardesty, R., Kofler, J. et al. (2013). Methane emissions estimate from airborne measurements over a western United States natural gas field, *Geophysical Research Letters*, 40 (16), 4393-4397. https://doi.org/10.1002/grl.50811

Katzenstein, A. S., Doezema, L. A., Simpson, I. J., Blake, D. R., & Rowland, F. S. (2003). Extensive regional atmospheric hydrocarbon pollution in the southwestern United States. *Proceedings of the National Academy of Sciences*, 100 (21), 11975-11979. https://doi.org/10.1073/pnas.1635258100

Kerr, T., & Yang, M. (2009). Coal mine methane in China: A budding asset with the potential to bloom. *IEA Information Paper*, 1-35.

Kirschke, S., Bousquet, P., Ciais, P., Saunois, M., Canadell, J. G., Dlugokencky, E. J. et al. (2013). Three decades of global methane sources and sinks. *Nature Geoscience*, 6 (10), 813-823. https://doi.org/10.1038/ngeo1955

Krautwurst, S., Gerilowski, K., Borchardt, J., Wildmann, N., Gałkowski, M., Swolkień, J. et al. (2021). Quantification of CH_4 coal mining emissions in Upper Silesia by passive airborne remote sensing observations with the Methane Airborne MAPper (MAMAP) instrument during the CO_2 and Methane (CoMet) campaign. *Atmos. Chem. Phys.*, 21 (23), 17345-17371. https://doi.org/10.5194/acp-21-17345-2021

Krautwurst, S., Gerilowski, K., Jonsson, H. H., Thompson, D. R., Kolyer, R. W., Iraci, L. T. ea al. (2017). Methane emissions from a Californian landfill, determined from airborne remote sensing and in situ measurements. *Atmos. Meas. Tech.*, 10 (9), 3429-3452. https://doi.org/10.5194/amt-10-3429-2017

Kuhlmann, G., Brunner, D., Emmenegger, L., Schwietzke, S., Zavala-Araiza, D., Thorpe, A. et al. (2023). Quantifying methane super-emitters from oil and gas production in Romania with the AVIRIS-NG imaging spectrometer. *EGU General Assembly 2023, Vienna, Austria, 24–28 Apr 2023*, EGU23-6751. https://doi.org/10.5194/egusphere-egu23-6751

Kuze, A., Suto, H., Nakajima, M.,& Hamazaki, T. (2009). Thermal and near infrared sensor for carbon observation Fourier-transform spectrometer on the Greenhouse Gases Observing Satellite for greenhouse gases monitoring. *Applied Optics*, 48 (35), 6716-6733.

https://doi.org/10.1364/AO.48.006716

Lauvaux, T., Giron, C., Mazzolini, M., d'Aspremont, A., Duren, R., Cusworth, D. et al. (2022). Global assessment of oil and gas methane ultra-emitters. *Science*, 375 (6580), 557-561. DOI: 10.1126/science.abj4351

Li, Q., Fernandez, R. P., Hossaini, R., Iglesias-Suarez, F., Cuevas, C. A., Apel, E. C. et al. (2022). Reactive halogens increase the global methane lifetime and radiative forcing in the 21st century. *Nature Communications*, 13 (1), 2768. https://doi.org/10.1038/s41467-022-30456-8

Li, X., Cohen, J. B., Qin, K., Geng, H., Wu, L., Wu, X. et al. (2023). Remotely Sensed and Surface Measurement Derived Mass-Conserving Inversion of Daily High-Resolution NO_x Emissions and Inferred Combustion Technologies in Energy Rich Northern China. *EGUsphere*, 2023, 1-30. https://doi.org/10.5194/egusphere-2023-2

Lin, B.-q., & Liu, J.-h. (2010). Estimating coal production peak and trends of coal imports in China. *Energy Policy*, 38 (1), 512-519. https://doi.org/10.1016/j.enpol.2009.09.042

Luther, A., Kleinschek, R., Scheidweiler, L., Defratyka, S., Stanisavljevic, M., Forstmaier, A. et al. (2019). Quantifying CH_4 emissions from hard coal mines using mobile sun-viewing Fourier transform spectrometry. *Atmos. Meas. Tech.*, 12 (10), 5217-5230. https://doi.org/10.5194/amt-12-5217-2019

Luther, A., Kostinek, J., Kleinschek, R., Defratyka, S., Stanisavljević, M., Forstmaier, A. et al. (2022). Observational constraints on methane emissions from Polish coal mines using a ground-based remote sensing network. *Atmos. Chem. Phys.*, 22 (9), 5859-5876. https://doi.org/10.5194/acp-22-5859-2022

Mehrotra, S., Faloona, I., Suard, M., Conley, S., & Fischer, M. L. (2017). Airborne Methane Emission Measurements for Selected Oil and Gas Facilities Across California. *Environmental Science & Technology*, 51 (21), 12981-12987. https://doi.org/10.1021/acs.est.7b03254

Miller, S. M., Michalak, A. M., Detmers, R. G., Hasekamp, O. P., Bruhwiler, L. M. P., & Schwietzke, S. (2019). China's coal mine methane regulations have not curbed growing emissions. *Nature Communications*, 10 (1), 303. https://doi.org/10.1038/s41467-018-07891-7

Molina, L. T., Madronich, S., Gaffney, J. S., Apel, E., de Foy, B., Fast, J. et al. (2010). An overview of the MILAGRO 2006 Campaign: Mexico City emissions and their transport and transformation. *Atmos. Chem. Phys.*, 10 (18), 8697-8760. https://doi.org/10.5194/acp-10-8697-2010

Peng, S., Piao, S., Bousquet, P., Ciais, P., Li, B., Lin, X., Tao, S. et al. (2016), Inventory of anthropogenic methane emissions in mainland China from 1980 to 2010. *Atmos. Chem. Phys.*, 16 (22), 14545-14562. https://doi.org/10.5194/acp-16-14545-2016

Plant, G., Kort, E. A., Murray, L. T., Maasakkers, J. D., & Aben, I. (2022). Evaluating urban methane emissions from space using TROPOMI methane and carbon monoxide observations. *Remote Sensing of Environment*, 268, 112756. https://doi.org/10.1016/j.rse.2021.112756

Povey, A. C., & Grainger, R. G. (2015). Known and unknown unknowns: uncertainty estimation in satellite remote sensing. *Atmos. Meas. Tech.*, 8 (11), 4699-4718. https://doi.org/10.5194/amt-8-4699-2015

Prather, M. J., Holmes, C. D., & Hsu, J. (2012). Reactive greenhouse gas scenarios: Systematic exploration of uncertainties and the role of atmospheric chemistry. *Geophysical Research Letters*, 39 (9). https://doi.org/10.1029/2012GL051440

Prinn, R., Cunnold, D., Rasmussen, R., Simmonds, P., Alyea, F., Crawford, A. (1987). Atmospheric Trends in Methylchloroform and the Global Average for the Hydroxyl Radical. *Science*, 238 (4829),

945-950. DOI: 10.1126/science.238.4829.945

Qin, K., Hu, W., He, Q., Lu, F.,& Cohen, J. B. (2023a). Individual Coal Mine Methane Emissions Constrained by Eddy-Covariance Measurements: Low Bias and Missing Sources. *EGUsphere*, 2023, 1-49. https://doi.org/10.5194/egusphere-2023-1210

Qin, K., Lu, L., Liu, J., He, Q., Shi, J., Deng, W. et al. (2023b). Model-free daily inversion of NO_x emissions using TROPOMI (MCMFE-NO_x) and its uncertainty: Declining regulated emissions and growth of new sources. *Remote Sensing of Environment*, 295, 113720. https://doi.org/10.1016/j.rse.2023.113720

Reuter, M., Buchwitz, M., Schneising, O., Krautwurst, S., O'Dell, C. W., Richter, A. et al. (2019). Towards monitoring localized CO_2 emissions from space: co-located regional CO_2 and NO_2 enhancements observed by the OCO-2 and S5P satellites. *Atmos. Chem. Phys.*, 19 (14), 9371-9383. https://doi.org/10.5194/acp-19-9371-2019

Rigby, M., Park, S., Saito, T., Western, L. M., Redington, A. L., Fang, X. et al. (2019). Increase in CFC-11 emissions from eastern China based on atmospheric observations. *Nature*, 569 (7757), 546-550. https://doi.org/10.1038/s41586-019-1193-4

Sadavarte, P., Pandey, S., Maasakkers, J. D., Lorente, A., Borsdorff, T., Denier van der Gon, H. et al. (2021). Methane Emissions from Superemitting Coal Mines in Australia Quantified Using TROPOMI Satellite Observations. *Environmental Science & Technology*, 55 (24), 16573-16580. https://doi.org/10.1021/acs.est.1c03976

Saunois, M., Stavert, A. R., Poulter, B., Bousquet, P., Canadell, J. G., Jackson, R. B. et al. (2020a). The Global Methane Budget 2000–2017. *Earth System Science Data*, 12 (3), 1561-1623. https://doi.org/10.5194/essd-12-1561-2020

Shi, T., Han, G., Ma, X., Mao, H., Chen, C., Han, Z. et al. (2023). Quantifying factory-scale CO_2/CH_4 emission based on mobile measurements and EMISSION-PARTITION model: cases in China. *Environmental Research Letters*, 18 (3), 034028. DOI: 10.1088/1748-9326/acbce7

Shi, T., Han, Z., Han, G., Ma, X., Chen, H., Andersen, T. et al. (2022). Retrieving CH_4-emission rates from coal mine ventilation shafts using UAV-based AirCore observations and the genetic algorithm–interior point penalty function (GA-IPPF) model. *Atmos. Chem. Phys.*, 22 (20), 13881-13896. https://doi.org/10.5194/acp-22-13881-2022

Tong, X., van Heuven, S., Scheeren, B., Kers, B., Hutjes, R., & Chen, H. (2023). Aircraft-Based AirCore Sampling for Estimates of N_2O and CH_4 Emissions. *Environmental Science & Technology*. https://doi.org/10.1021/acs.est.3c04932

Tu, Q., Hase, F., Schneider, M., García, O., Blumenstock, T., Borsdorff, T. et al. (2022). Quantification of CH_4 emissions from waste disposal sites near the city of Madrid using ground- and space-based observations of COCCON, TROPOMI and IASI. *Atmos. Chem. Phys.*, 22 (1), 295-317. https://doi.org/10.5194/acp-22-295-2022

Varon, D. J., Jacob, D. J., McKeever, J., Jervis, D., Durak, B. O. A., Xia, Y., & Huang, Y. (2018). Quantifying methane point sources from fine-scale satellite observations of atmospheric methane plumes. *Atmos. Meas. Tech.*, 11 (10), 5673-5686. https://doi.org/10.5194/amt-11-5673-2018

Vaughn, T. L., Bell, C. S., Pickering, C. K., Schwietzke, S., Heath, G. A., Pétron, G. et al. (2018). Temporal variability largely explains top-down/bottom-up difference in methane emission estimates from a natural gas production region. *Proceedings of the National Academy of Sciences*, 115 (46), 11712-11717. https://doi.org/10.1073/pnas.1805687115

Vinković, K., Andersen, T., de Vries, M., Kers, B., van Heuven, S., Peters, W. et al. (2022). Evaluating

the use of an Unmanned Aerial Vehicle (UAV)-based active AirCore system to quantify methane emissions from dairy cows. *Science of the Total Environment*, 831, 154898. https://doi.org/10.1016/j.scitotenv.2022.154898

Wecht, K. J., Jacob, D. J., Sulprizio, M. P., Santoni, G. W., Wofsy, S. C., Parker, R. et al. (2014). Spatially resolving methane emissions in California: constraints from the CalNex aircraft campaign and from present (GOSAT, TES) and future (TROPOMI, geostationary) satellite observations. *Atmos. Chem. Phys.*, 14 (15), 8173-8184. https://doi.org/10.5194/acp-14-8173-2014

Zhang, Y., Gautam, R., Pandey, S., Omara, M., Maasakkers, J. D., Sadavarte, P. et al. (2020). Quantifying methane emissions from the largest oil-producing basin in the United States from space. *Science Advances*, 6 (17), eaaz5120. https://doi.org/10.1126/sciadv.aaz5120

Figures

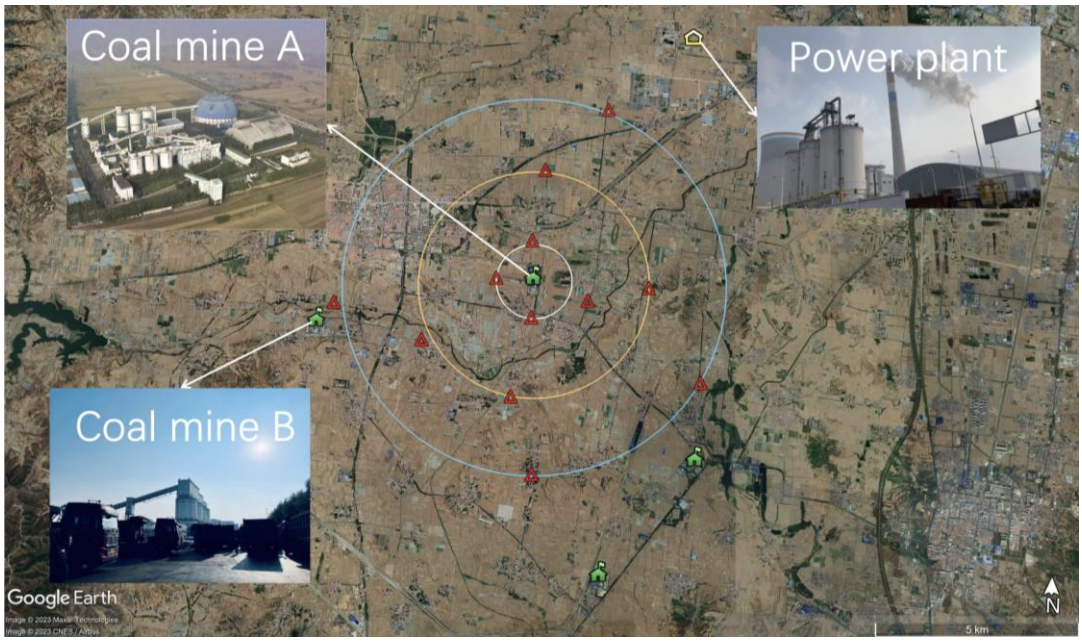

Figure 1. Locations of four individual coal mines (Green filled houses), a power plant (Yellow outlined house), and the 12 observation locations presented in this work (red double-outlined triangles). Distance from CM-A are given as concentric circles at 1km (white), 3km (yellow), and 5km (blue).

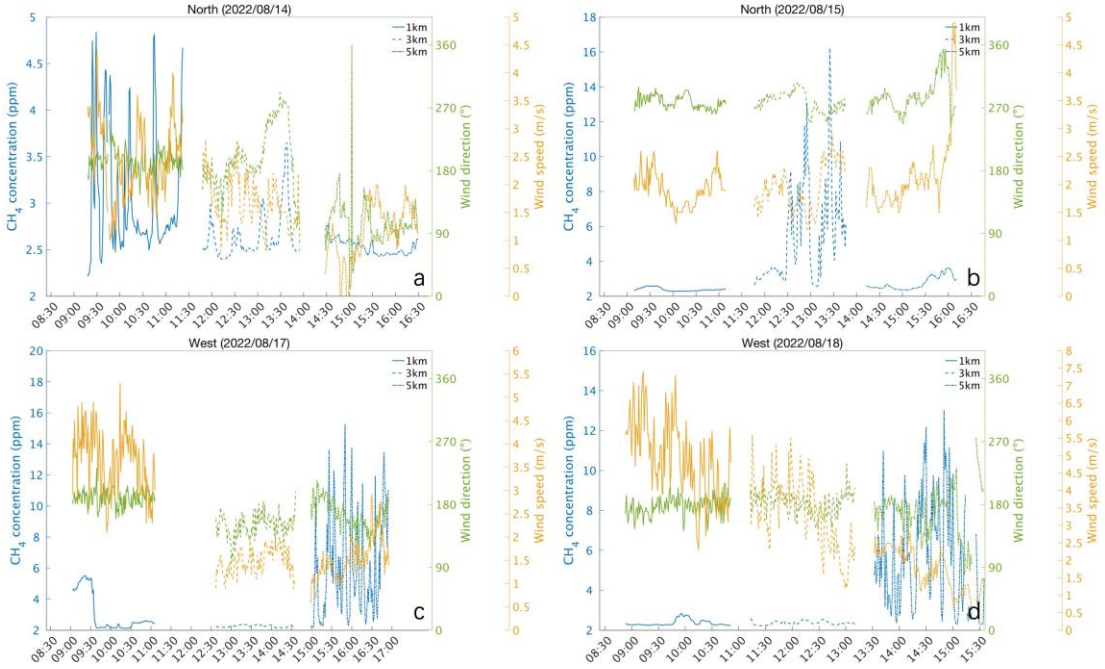

Figure 2. Time series of CH_4 concentration [ppm] (blue), wind speed [m/s] (yellow) and wind direction [°] (orange lines) measured at 1km (solid), 3km (dashed) and 5km (dash-dot) located north (top) and west (bottom) of CM-A on four different days (August 14 top left, August 15 top right, August 17 bottom left, and August 18 bottom right).

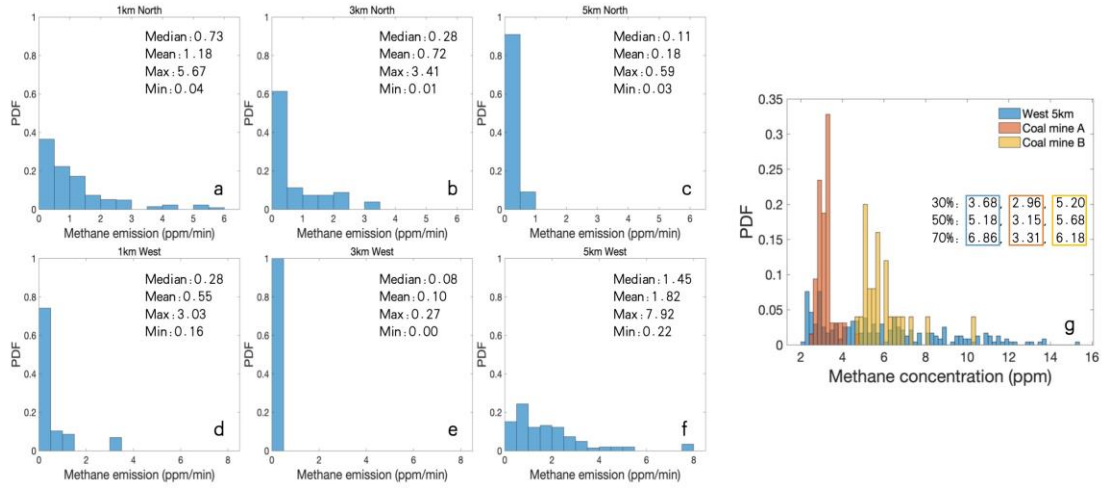

Figure 3. Probability density functions [PDF] of computed CH_4 emissions located at 1km north (a), 3km north (b), 5km north (c), 1km west (d), 3km west (e), and 5km west (f) of CM-A, including median, mean, maximum, and minimum statistics. The PDFs of CH_4 concentration measured at 5km west (blue) and simulated using the 2-Box model under conditions when the source is CM-A (red), and when the sources is CM-B (orange), including representative 30%, 50%, and 70% bounds are in (g).